Solar Energy Materials & Solar Cells 117 (2013) 145–151

Contents lists available at ScienceDirect

Solar Energy Materials & Solar Cells

journal homepage: www.elsevier.com/locate/solmat

A look into the origin of shunt leakage current of Cu(In,Ga)Se_2 solar cells via experimental and simulation methods

Yu-Kuang Liao [e], Shou-Yi Kuo [b,*], Ming-Yang Hsieh [b], Fang-I Lai [c,f], Ming-Hsuan Kao [a], Shun-Jen Cheng [e], Ding-Wen Chiou [d], Tung-Po Hsieh [d], Hao-Chung Kuo [a]

[a] Department of Photonics and Institute of Electro-Optical Engineering, National Chiao Tung University, Hsinchu 30010, Taiwan, ROC
[b] Department of Electronic Engineering, Chang Gung University, Taiwan, ROC
[c] Department of Photonic Engineering, Yuang Ze University, Taoyuan, Taiwan, ROC
[d] Compound Semiconductor Solar Cell Department, Next Generation Solar Cell Division, Green Energy and Environment Research Laboratories, Industrial Technology Research Institute, Hsinchu, Taiwan, ROC
[e] Department of Electro-physics, National Chiao Tung University, Taiwan, ROC
[f] Advanced Optoelectronic Technology Center, National Cheng Kung University, Taiwan, ROC

ARTICLE INFO

Article history:
Received 4 May 2012
Received in revised form
15 April 2013
Accepted 11 May 2013
Available online 21 June 2013

Keywords:
CIGS
Space-charged limited current
Dark current
Shunt leakage
APSYS
Temperature dependence *IV*

ABSTRACT

This study investigates how to apply space-charge-limited (SCL) current to describe shunt leakage current in a CIGS solar cell. Possible factors inducing SCL current have been observed through conductive atomic force microscopy (C-AFM), which supports the SCL current theory, describing the shunt current of a CIGS solar cell. In simulations derived from experimental data, deviation of dark *IV* curves is due to flaws in the real device. These flaws are absent in simulation, but investigation verifies the characteristics of SCL current component's experimental *IV* curves within shunt leakage current. A device with a metal/CIGS/metal structure could simulate SCL current and confirm its characteristics. Such a simulated structure, representing flaws inserted into a CIGS solar cell, generates the same dark-current behavior revealed in experimental dark *IV* curves. This study investigates the response of dark current to varying sizes of the flaw within the CIGS solar cell.

1. Introduction

Conventional crystalline silicon solar cells are expensive because of the tremendous cost of fabricating silicon wafers. Thin-film solar cells reduce the cost of PV merchandise yet the limited efficiency of thin-film solar cells is a great challenge in the new energy industry. A breakthrough of 20.3% in efficiency has been achieved with ternary chalcopyrite material Cu(In,Ga)Se_2 (CIGS)-based solar cells [1]. This offers cost efficiency, irradiative stability, and adaptability to versatile applications [2,3]. Such advantages provide CIGS solar cells with high potential for an effective solution to global warming and energy issues.

Electronic loss of current transporting through interfaces in a delicate device structure has always been a problem with thin-film technologies. It has hampered improvement of thin-film CIGS solar cells. Related issues to current loss are a common difficulty throughout thin film technologies since the quality control of devices constructed with thin films with thickness in micrometers, or even in nanometers, is always a big challenge during fabrication when coming to the commercial needs in high throughput of large area devices [4]. In the case of CIGS solar cells, CIGS surface roughness and thin ZnO/CdS layers (50–100 nm) covering the CIGS layer could cause shunt leakage current due to locally bad coverage. In an equivalent solar-cell circuit, it is a conventional way to treat shunt leakage current as an Ohmic current. However, in the case of thin-film solar cells, including CIGS solar cells, this assumption is not always correct [5].

Space charge limited (SCL) current theory has been used to generalize the mechanism of shunt current in various kind of thin film solar cells [6]. The SCL current theory, a theoretical physics model, describes current being driven into an insulator, i.e. a current flowing through a device with structure of metal/insulator/metal. The expression of SCL current density has been derived as [7]

$$J_{SCL} = \mathrm{sgn}(V) q \mu N_V \left(\frac{s}{qN_t}\right)^l \frac{|V|^{l+1}}{d^{2l+1}} \quad (1)$$

where "sgn" is the sign function, ε is the dielectric constant of the insulator or the semiconductor, μ is the effective mobility of holes in CIGS case, and I is T_c/T of which T_c is the characteristic temperature of an exponential trap distribution in a form of $N_t \propto e^{(-E/K_B T_c)}$ and E in

* Corresponding author. Tel.: +886 3 2118800.
E-mail addresses: sykuo@mail.cgu.edu.tw (S.-Y. Kuo), hckuo@faculty.nctu.edu.tw (H.-C. Kuo).

0927-0248/$ - see front matter © 2013 Elsevier B.V. All rights reserved.
http://dx.doi.org/10.1016/j.solmat.2013.05.031

the exponent is the energy level measured from the valence band. The description of SCL current shows a symmetric *IV* curve about $V=0$. In particular, this description also illustrates the insensitivity to temperature of SCL current since the only physical parameter depending on temperature is hole mobility μ—a weak function of temperature. Under SCL current model assumptions, formation of shunt current in a CIGS solar cell is due to local interconnection between absorption layer and Al cluster in the AZO layer, invading through the extremely thin ZnO/CdS layers. Such Al clusters will allow the passage of injected carriers supposedly forbidden under reverse bias voltage. In such cases, a metal/insulator/metal band structure, suggested in the SCL current theory, forms and contributes to shunt current.

Mott and Gurney [8] discovered that trap energy levels within the forbidden gap of insulators could locally confine injected carriers from current. This results in formation of "space-charge" distribution among the insulator, limiting the magnitude of injected current. Rose's [9] and Lampert's [7] detailed depiction of the SCL current theory during the fifties and the sixties had characterized SCL current well. In this work, we intended to investigate into the adaptability of SCL current model to shunt leakage in a CIGS solar cell.

To generate SCL current, the injected carriers must be controlled as one single type. This ensures that the host material, e.g., the insulator or semiconductor, is filled with one excess carrier that avoids neutralization. Neutralization can suppress the limitation of injected current determined by space-charge if electrons and holes are simultaneously injected into the host material. Holes, in the case of CIGS solar cells, must be the only contribution to SCL current undergoing within a structure of metal/CIGS/metal. Abundant defects in CIGS with energy levels located within the forbidden gap have been observed. Defects act like donors and acceptors, dominating CIGS electrical characteristics [10]. Those defect levels could confine carriers and form space-charge where current is injected (Fig. 1). P-type CIGS characteristics form a band alignment that builds up a great potential barrier for electrons, potentially driven into CIGS and a rather smaller one for holes tending to be driven in the same way. A p-type CIGS possesses a higher concentration of acceptor-like defects than that of donor-like defects, hence the contribution of space charge is from holes trapped by those acceptor-like defects (Fig. 1). There might be a small amount of copper-rich secondary phases existing in absorber layer of a CIGS solar cell effecting on the behavior of shunt leakage, yet, due to that an absorber layer for a CIGS solar cell with reasonably good efficiency needs to be copper-poor, therefore the amount of secondary phases is very small and its effect on shunt leakage is ignorable.

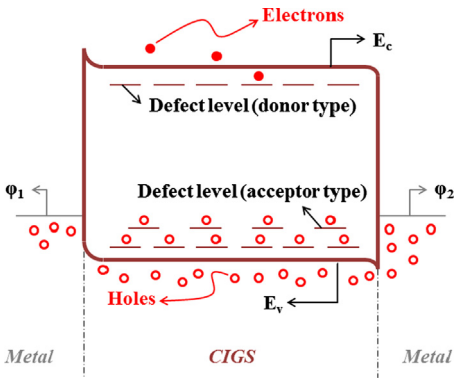

Fig. 1. Schematic band diagram for single carrier injection in metal/CIGS/metal structure, in which E_c and E_v are energies at conduction band edge and valence band edge, φ_1 and φ_2 are work functions of metals at the two ends. The diagram indicates the condition that allows formation of SCL current in CIGS, in which only holes can easily go through CIGS bulk and are limited by space-charge formed by holes itself trapped at defect in CIGS bulk.

This study examines possible current paths of shunt leakage through ZnO/CdS layers utilizing conductive atomic force microscopy (C-AFM), and investigates the behavior of shunt leakage through a temperature-dependent dark-current voltage measurement (dark TD-*IV*) of a CIGS solar cell. It simulates dark current and compares the results to experimental data, extracting shunt leakage behavior from the whole. Extraction is possible through applying an SCL current model after examining suitable adaptation of SCL current model to shunt leakage. This study then investigates the change in shunt leakage current under different levels of metal incursion into device's CIGS layer. The CIGS absorber layer's band diagram was constructed according to the Ga gradient concentration observed through a Time-of-Flight Secondary Ion Mass Spectrometer (TOF-SIMS) to meet the actual form of CIGS bandgap.

2. Experiments and simulations

A CIGS solar cell on soda lime glass (SLG) with ZnO:Al (AZO)/ZnO/CdS/CIGS/Mo/SLG structure has been prepared through a three-stage co-evaporation process. The absorber layer in the device has a resultant [Ga]/[Ga]+[In] (GGI) ratio around 0.3 and a [Cu]/[In]+[Ga] ratio around 0.7. The n-type CdS layer was deposited by chemical bath deposition while the i-ZnO layer and AZO layer were deposited by the RF sputtering method. The thicknesses of Mo, CIGS, CdS, i-ZnO and AZO were 800 nm, 2 μm, 50 nm, 50 nm and 250 nm, respectively. Efficiency measurements were performed, closely following the procedure described in international standard CEI IEC 60904-1. Both the solar cells and the reference cell were characterized under a simulated Air Mass 1.5, Global (AM1.5G) illumination [11] with a power of 1000 W/m^2. The temperature was actively controlled during the measurements and was 25 ± 1 °C. The power conversion efficiency (PCE) measurement system consisted of a power supply (Newport 69920), a 1000 W Class A solar simulator (Newport 91192 A) with a Xenon lamp (Newport 6271 A) and an AM1.5G filter (Newport 81088 A), a probe stage, and a source-meter with a four-wire mode (Keithley 2400). In the calibration report by Newport Corporation, the temporal instability was 0.88%, and the non-uniformity was 0.79%. The spectrum of the solar simulator was measured by a calibrated spectroradiometer (Soma S-2440) in the wavelength range of 300 nm–1100 nm. Before measurement, the intensity of the solar simulator was calibrated by a mono-crystalline silicon reference cell with a 2 cm × 2 cm illumination area (VLSI Standards, Inc.) [12]. The CIGS solar cell's efficiency was 12%. All dark *IV* measurement was conducted using the same integrated equipment without illumination. Two as-deposited samples were simultaneously prepared. One has a structure of ZnO/CdS/ITO Glass for C-AFM (NT-MDT Solver P47, SP-47) measurements under a bias voltage of 1 V. A corner of ITO layer was exposed without for electrode contact while C-AFM measurement. The other as-deposited sample had a structure of CIGS/Mo/SLG for TOF-SIMS (ION-TOF TOF-SIMS *IV*) measurements. The software used for simulation was Crosslight APSYS. APSYS is based on 2D finite element analysis and Poisson equation approach, drift-diffusion model to analyze electrons and holes transportation for structure of photovoltaic devices. The device structure in simulations was deliberately constructed to be identical to the actual investigated CIGS solar cell. Fig. 2(a) and (b) demonstrates the device structure and the band diagram of the device established in simulation, respectively. In Fig. 2(b), the black line and red line represent the conduction band and the valence band respectively, while the blue line labels the Fermi level. The V-shaped conduction band edge of

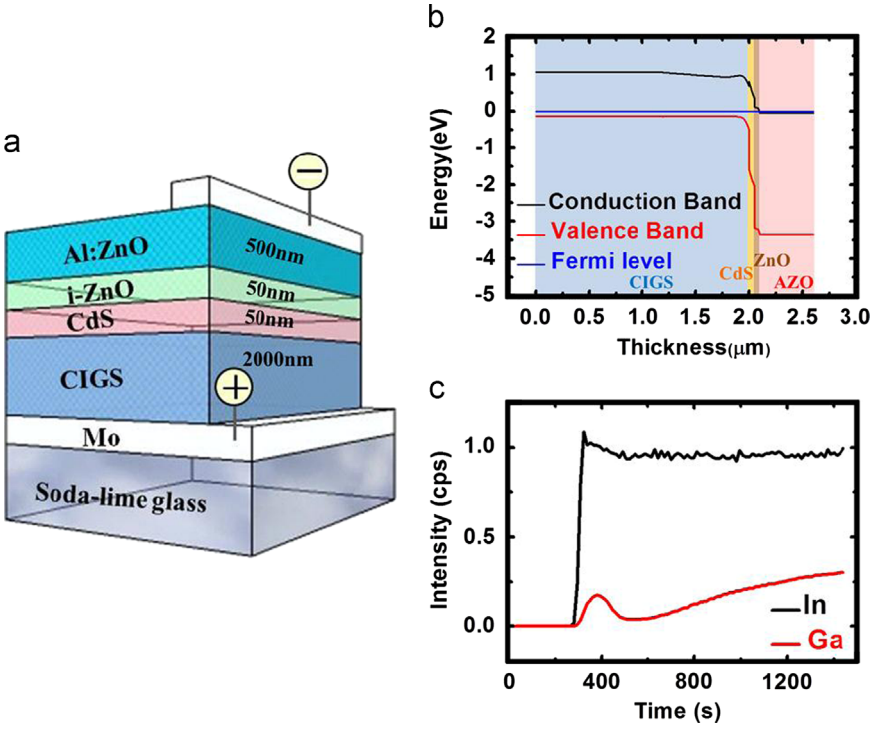

Fig. 2. Schematic description of (a) the structure of the CIGS solar cell investigated in this study and (b) the band diagram of the CIGS solar cell established in simulation. The latter was constructed according to (c) the experimental SIMS depth profile of In and Ga of an as-deposited CIGS thin film while preparing the investigated CIGS solar cell.

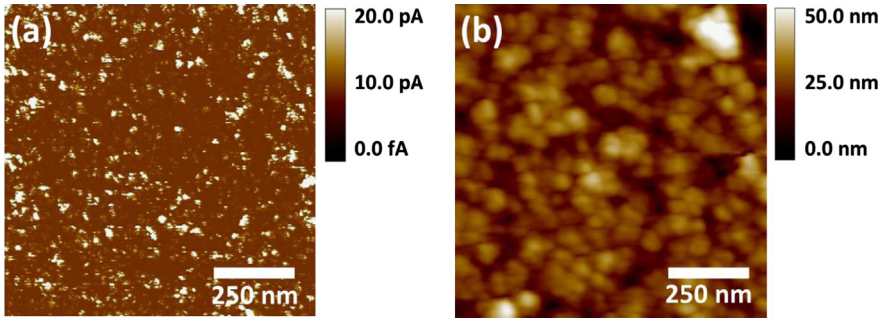

Fig. 3. (a) The C-AFM image of the ZnO/CdS/ITO Glass sample and (b) its corresponding AFM image obtained by scanning the same area on the sample where the CAFM image was obtained. The scanned area was chosen to be 1 μm to match the general grain size of polycrystalline CIGS thin film for demonstration of a total potential contribution of leakage path that forms SCL current.

CIGS nearby the CIGS/CdS interface shown in Fig. 2(b) was based on the resultant SIMS diagram of CIGS absorber layer (Fig. 2[c]). A V-shaped band diagram of CIGS can be achieved through a gradient concentration of Ga dopant varying upon depth and is a conventional way to enhance light absorption as well as a better carrier extraction in a CIGS solar cell [13–15].

3. Results and discussions

SCL current is not expected in a device with an asymmetric structure and built-in potential, as that of a CIGS solar cell. SCL current is supposed to be observed in a device with structure of metal/insulator/metal [9]. Such structure can be locally formed in a CIGS solar cell and results in the absence of built-in potential where enhancement of shunt current behaving as SCL current is present. This could be caused by locally poor coverage of the CdS and ZnO layers on CIGS. In the band diagram shown in Fig. 2(b), one can see the thin gap between CIGS and AZO caused by CdS and ZnO buffer layers with total thickness of 100 nm and the potential barrier blocking holes transporting from CIGS layer toward the other end. If metal clusters, say, Al in the AZO layer, invade the CIGS layer due to locally bad coverage of ZnO, and CdS hence forms a "metal bridge" connecting to electrodes, they eliminate the barrier for holes and the symmetric band structure providing SCL current will be formed. AZO thin films prepared under room temperature using the RF magnetron sputtering technique have poor crystallinity and a smaller average grain size than those of AZO thin films prepared under a higher temperature. Low mobility of deposited atoms and weak diffusion of Al atoms during deposition caused poor occupation probability of Al ions on Zn sites [16]. Self-aggregation of Al clusters may consequently occur. It could likely be happening in a CIGS solar cell that has an AZO layer deposited under room temperature as transparent conductive oxide layer, as the one examined in this study. With an Al cluster, once a CdS layer performs poor local coverage on CIGS, Al clusters may be squeezed into such flaws, contributing to SCL current. C-AFM checks for such possible contributions.

The C-AFM images of the as-deposited sample, fabricated into a structure of ZnO/CdS/ITO Glass (Fig. 3), reveal the existence

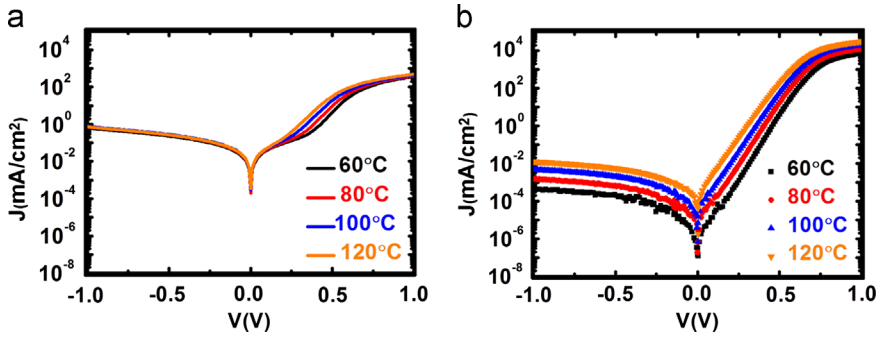

Fig. 4. (a) The experimental dark current–voltage curves of the CIGS solar cell with efficiency of 12% taken under device temperature of 60 °C, 80 °C, 100 °C, and 120 °C and (b) the simulated dark current–voltage curves of a CIGS solar cell similarly taken under device temperature of 60 °C, 80 °C, 100 °C and 120 °C. The comparison of results in experiments showed in (a) and the results showed in simulation showed in (b) indicates the contribution of SCL current appeared in experimental data which is absent in simulation.

of locally poor coverage of CdS and ZnO. Fig. 3(a) shows the C-AFM images while Fig. 3(b) displays the corresponding AFM images. The white dots on the C-AFM images represent detected current. Abundant leakage current contribution is clear from the C-AFM image. The same measurement on another as-deposited CIGS thin film was integrated into the structure of CdS/CIGS/Mo/ITO Glass (not shown here). Without the capping of a highly-resistive ZnO layer on top, the leakage current contribution is even more vigorous. From the AFM image, one can see the rough surface of the 50 nm-thick CdS layer with ZnO capping. It reveals a grain size around 100 nm, and local roughness variation up to 50 nm, which is the thickness of CdS, can be observed. They reveal the lack of sample homogeneity and possible locations with a weaker built-in potential. Those locations prove the actual formation of imperfect structure which can induce SCL current during contact with a metal cluster. SCL current component can thus be easily observed from dark *IV* curves of a CIGS solar cell. In order to confirm the existence of SCL current, the fastest way is to actually check the experimental dark *IV* curves of a CIGS solar cell.

Characteristics of SCL current emerge in experimental dark *IV* curves. Fig. 4(a) shows the dark current dark TD-*IV* curves of the CIGS solar cell under 60 °C, 80 °C, 100 °C and 120 °C. According to Ref. [6] one can treat the reverse current as shunt leakage current. The SCL current theory may characterize this as the contribution of diode current, nearly eliminated by a built-in potential conflicting with transporting carriers under reverse-bias voltage. The theory indicates that the SCL current is a weak function of temperature. Using the SCL current model, Fig. 4(a) indicates that the reverse current shows extreme insensitivity to temperature at all applied voltages. The consistence has demonstrated the adaptation of SCL current model to shunt current. For forward current, one can treat it as the sum of shunt current (which is insensitive to temperature) and diode current (which is more sensitive to temperature) [6]. The forward current curves in Fig. 4(a) show that current behavior is insensitive to temperature under low applied voltage, but is more sensitive to temperature with larger applied voltage. This fact can be understood as the domination of shunt current under lower applied voltage and the “overtaking” of diode current under larger applied voltage. A bend is also observed at the right end of forward current curves. This is caused by series resistance of the device, which starts to play a role when the current flowing through the device becomes larger. It induces an additional reverse electromotive force exerting against applied voltage and hence reduces the forward current. This makes the current behavior more similar to SCL current since the diode current component is reduced [17]. The temperature-dependent behavior of dark current in Fig. 4(a) is consistent with the shunt current model based on the SCL current theory.

Simulation results from dark temperature-dependent *I–V* measurements of a CIGS solar cell indicate otherwise (Fig. 4[b]). Sensitivity to temperature of the dark *IV* curves is equally evident at every applied voltage. Slight insensitivity emerges at high forward applied voltage larger than 0.7 V. The suppression of sensitivity to temperature under applied voltage above 0.7 V is due to series resistance which greatly reduces forward current under high applied voltage at all temperatures. The effect of series resistance is observable in the experimental dark temperature-dependent *I–V* curves (Fig. 4[a]). Conversely, the consequent general temperature sensitivity results from simulation under all applied voltages have come into conflict against the experimental outcomes. In Fig. 4(b), the reverse current obviously increases with the rising temperature, whereas in Fig. 4(a), almost no consequent change with varying temperature is evident from the reverse current. The reverse current density in experimental data (Fig. 4 [a]) is substantially larger than that of the simulation (Fig. 4[b]). It can be understood as, in Fig. 4(a), an additional shunt current, which is large and SCL-current like, has appeared and quenched the diode current, hence causing temperature-insensitive behavior. As for simulation, since no metal incursion had been constructed in the device model used to simulate dark temperature-dependent *I–V* curves (Fig. 4[b]), the dark *IV* curves only shows the behavior of diode current and therefore is sensitive to temperature. The way the experimental results have deviated from that of simulation has strongly implied the current component of SCL current within. To understand how the SCL current model can explain shunt current in a CIGS solar cell, this study simulates a device structure particularly involving CIGS participation that could precisely generate SCL current. It also simulates a structure of a CIGS solar cell with metal incursion for comparison.

A device with a metal/CIGS/metal structure was constructed in simulation. Fig. 5(a) shows its band diagram while the inset shows its structure. The figure shows a stack piled up with layers of metal/CIGS/metal from the inset. The electrodes were set to connect to the two metallic ends. This structure was intentionally built to consist with the description in the theory of SCL current. The band diagram in Fig. 5(a) shows a band alignment needed to generate SCL current such as that suggested in Fig. 1. The energy level of work function belonging to the two metallic ends on both sides is very close to the energy level of the CIGS valence band. A condition of single-carrier injections needed for SCL current can easily happen since the interface barrier between CIGS and metal for holes is much smaller than that for electrons. The V-shaped CIGS band diagram is also intentionally structured to coincide with the actual shunt path in reality, which is shown in Fig. 2. Once metal incursion occurs, such band structure is what to be observed as a shunt path in a CIGS solar cell.

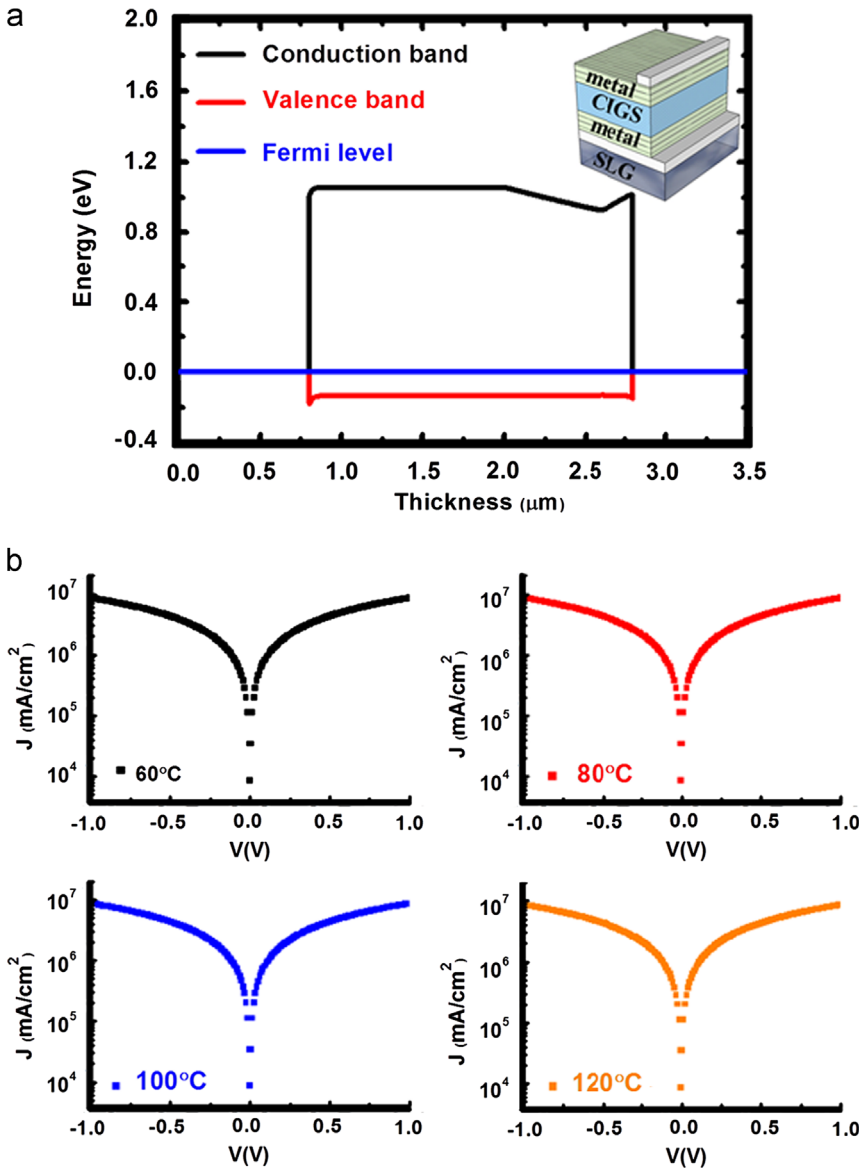

Fig. 5. (a) The schematic band diagram of the metal/CIGS/metal device used in simulation. The inset shows the structure of the device used to obtain the shown band diagram in simulation. (b) The dark current–voltage curves of metal/CIGS/metal device taken under device temperature of 60 °C, 80 °C, 100 °C and 120 °C obtained by simulation.

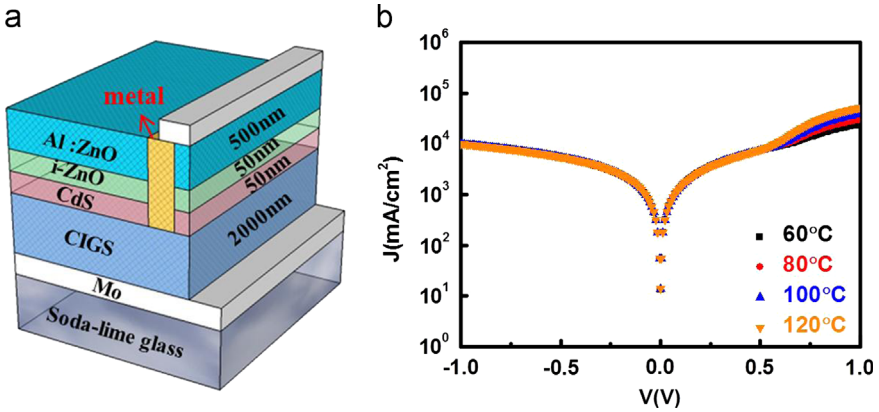

Fig. 6. (a) The simulated structure of a CIGS solar cell with flaw of metal incursion. (b) The dark current–voltage curves of the CIGS solar cell with metal incursion under 60 °C, 80 °C, 100 °C and 120 °C obtained by simulation using the shown simulated structure with metal incursion.

Fig. 5(b) shows the results of simulated *IV* curves under 60 °C, 80 °C, 100 °C, and 120 °C conditions. In the figure, all *IV* curves under different temperatures exhibit a symmetric dependence with respect to an applied voltage approximates $V=0$, which agree with the *IV* relation of SCL current (Eq. [1]). *IV* curves are completely identical under all temperatures. The characteristics

of temperature independence and symmetry about $V=0$ coincide with the theoretical illustration of SCL current. The result of the temperature independence *IV* curves of the metal/CIGS/metal device implies insensitivity to temperature of reverse current, exhibited in the experimental *IV* curves (Fig. 4[a]). A constant hole mobility μ used in simulation may be the cause of complete invariance to temperature of the *IV* curves (Fig. 5[b]). Furthermore, the behavior of *IV* curves under all temperatures in simulation shown in Fig. 5(b) well consists with the theoretical description of SCL current illustrated in Ref. (7). These facts have showed that the metal/CIGS/metal structure is able to generate SCL current and also strongly inferred that the shunt leakage current can be characterized by the SCL current model. The significant magnitude of current shows the possibility of that even a small amount of metal incursion can lead to large shunt leakage current.

Fig. 6(a) shows the structure of the constructed CIGS solar cell with a flaw of metal incursion within the device. The structure is exactly identical to that shown in Fig. 2(a), except for a metal slab penetrating through AZO, ZnO and CdS layer which contacts with CIGS layer at the bottom and front electrode on the top representing a condition of metal incursion. A metal gap is therefore formed with the inserted metal slab. The ratio of the width of the gap to that of the entire device is $1:10^6$. Once the holes generated in CIGS have been captured by the metal and been confined inside the metal slab, these holes will be taking a transportation path that is built with CIGS connecting with metal on its two ends which is the metal/CIGS/metal structure (inset of Fig. 5[a]).

Fig. 6(b) shows the simulated dark *IV* curves under 60 °C, 80 °C, 100 °C and 120 °C of the device with metal incursion. There is a great difference between the simulated *IV* curves obtained from a CIGS solar cell with metal incursion (Fig. 6[b]) and that without metal incursion (Fig. 6[b]). Comparing with the simulated dark *IV* curves of the CIGS solar cell without metal incursion, one can see that the dark current of that with metal incursion is a lot more appreciable in which the magnitude of itself mostly stay between 103 and 104 mA/cm^2. Another great difference between the CIGS solar cell with and without metal incursion in simulation is that the dark *IV* curves simulated from that with metal incursion generally show irrelevance to temperature. An exception occurs when a forward bias voltage larger than 0.6 V is applied: another current contribution varying with temperature emerges and results in a splitting of these dark *IV* curves. This current contribution has a magnitude (104–105 mA/cm^2) close to that obtained from the CIGS solar cell in simulation without metal incursion in the same range of applied voltage. Metal incursion changes the dark *IV* curves of a CIGS solar cell by bringing SCL current into the global contribution of dark current. The dark current (Fig. 6[b]) is a summation of diode current, which has the characteristics exhibited in Fig. 4(b), and SCL current, which has the characteristics exhibited in Fig. 5(b).

Much like the observations of dark *IV* curves shown in Fig. 4(a), diode current and SCL current separately dominated in different ranges of applied voltage. When the absolute value of applied voltage was below 0.6 V, a certain amount of carrier injected into the CIGS solar cell with metal incursion "leaked" into the metal flaw and contributed to SCL current component. The leaked carrier was supposed to be mostly "blocked away" by the built-in potential at the p–n junction. The two corresponding figures show that, within this range of applied voltage, the shunt leakage had brought about a larger current than that of the flawless CIGS solar cell exerted with the same magnitude of applied voltage. It behaved consistently with the characteristics of SCL current displayed in Fig. 5(b). This is the reason why the schematic illustrations of the change in these dark *IV* curves were all traced out symmetrically about $V=0$ and insensitive to temperature under lower applied voltages; this was not observed in the *IV* curves of the CIGS solar cell without metal incursion (Fig. 4[b]). When the absolute value of applied voltage had exceeded 0.6 V, the individual outcomes of that under forward bias voltage and that of under reverse bias voltage had been distinguished. Under this condition, the reverse current continued to obey the principles defining SCL current. The diode current was still suppressed by a built-in potential in an even extended space-charge region blocking away the transporting carriers contributing to diode current. The SCL current therefore overwhelmed it. As for the forward current within this range of applied voltage, the diode current was large enough to surpass SCL current in magnitude. The emergence of diode current meant the forward current no longer behaved like SCL current. This brought out the characteristics of diode current, including the sensitivity to temperature. A fact that the emerged forward diode current shown in Fig. 6(b) has a magnitude close to that shown in Fig. 4(b) under the same range of forward bias voltage illustrates that, even for a CIGS solar cell having flaws of metal incursion, the behavior of forward current under such a large forward bias voltage is similar to that of the CIGS solar cell without metal incursion (Fig. 4[b]). Under a forward bias voltage larger than 0.6 V, most of the injected carriers have energy large enough to break through the space-charge region so that the diode current can freely contribute to dark current. Since metal incursion only occupies a tiny part of the flawed CIGS solar cell, the SCL current becomes irrelevant and results in the dominance of diode current. The perspective of dividing dark current into diode current and SCL current has likewise been applied to analyze the experimental dark *IV* curves, shown in Fig. 4(a). The two current components shown in Fig. 4(a) exhibit good consistency with all illustrated analytic descriptions of *IV* curves obtained through a simulation shown in Fig. 6(b).

Different levels of measuring the contribution of metal incursion have been adapted to a simulation of dark current of a CIGS solar cell: a CIGS solar cell with a metal gap (Fig. 6[a]) that has various widths in which the metal gap represents metal incursion. Different widths of the metal gap give different volumes of metal incursion in the device. The different ratios of the width of metal gap to that of the entire device were set to be $1:10^6$ and $1:10^5$ that were to compare the outcomes of themselves to that of a device with metal/CIGS/metal structure. All curves were obtained under 100 °C. The characteristic of diode current was easily quenched by the aggressively growing SCL current as the metal gap widened (Fig. 7). Diode current can still be seen under a high forward bias voltage when the ratio measuring the level of metal incursion was $1:10^6$. As the ratio was altered to $1:10^5$, even under a large forward bias voltage, diode current was no longer being able to be observed. As the metal gap widened to the condition of metal/

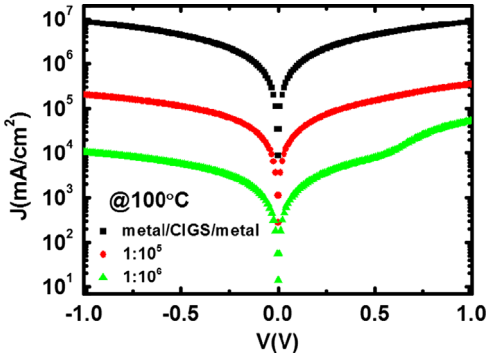

Fig. 7. The simulated dark current–voltage curves under 100 °C of a CIGS solar cell with different areas of metal incursion and with the dark current–voltage curves of the metal/CIGS/metal device under 100 °C. For the simulated CIGS solar cells with different areas of metal incursion, the ratios of the width of metal incursion to that of the entire device used in simulation are $1:10^6$ and $1:10^5$.

CIGS/metal, the current was gradually raised to match the dark *IV* curve under 100 °C (Fig. 5[b]). Because the simulation was conducted using a two-dimensional model, one can maintain the illustrated schematic device structure in the two dimensions where it is laid out, extending it along the third dimension to a reasonable length to construct a three-dimensional device. According to the pictured image of the three-dimensional device, the area of metal incursion could represent a value of tens of square micrometers. This is substantially larger than that possible in a CIGS solar cell. Therefore, SCL characteristics are clear in simulations of this study. According to the rapid rate of which the magnitude of current was raised with the widening metal gap, metal incursion could severely induce shunt current.

4. Conclusion

This work investigates how SCL current can describe shunt current of a CIGS solar cell. From the C-AFM image of a sample with structure of ZnO/CdS/ITO Glass, the existence of contributions to SCL current can demonstrably allow metal clusters of the AZO layer. These could penetrate through ZnO and CdS layers right into CIGS layer and induce shunt current. A model of CIGS solar cell through simulation, based on the experimental outcome of TOF-SIMS, has been applied to a CIGS thin film of which an as-deposited thin film CIGS was fabricated into a CIGS solar cell (efficiency of 12%). This study compares the results obtained from simulation to experimental *IV* curves of the 12%-efficiency CIGS solar cell. An additional shunt current that has characteristics of SCL current is observable from the experimental *IV* curves, whereas it has not been observed in the *IV* curves obtained from simulation. Those flaws in the CIGS solar cell were intentionally not set up in the simulation. Researchers then constructed a device with structure of metal/CIGS/metal through a simulation and confirmed the characteristics of SCL current, showing the temperature independence and symmetry with respect to an applied voltage approximates $V=0$. Such a structure yields the contribution of shunt current that a CIGS solar cell constructed in simulation. A metal gap partly forms a structure of metal/CIGS/metal in the device. The resultant *IV* curves under all temperatures are the summation of diode current and SCL current. The two current components have individually exhibited their corresponding current characteristics in simulation, as has been similarly observed in experimental *IV* curves. The SCL current also rapidly increases as the metal gap widens, implying that tiny area of metal incursion can still induce appreciable SCL current.

Acknowledgments

The authors would like to thank Compound Semiconductor Solar Cell Department, Next Generation solar cell Division, Green Energy and Environment Research Laboratories, Industrial Technology Research Institute of Taiwan for technical supports. This work was supported by the Green Technology Research Center of Chang Gung University and the National Science Council (NSC) of Taiwan under contract nos. : NSC-100–3113-E-182 -001-CC2 and NSC-100–2112-M-182-004. Funding for this work was also provided by (Department of Industrial Technology) Ministry of Economics Affairs, Taiwan. Contract No.102-EC-17-A-02-02-0756.

References

[1] P. Jackson, D. Hariskos, E. Lotter, S. Paetel, R. Wuerz, R. Menner, W. Wischmann, M. Powalla, New world record efficiency for Cu(In,Ga)Se_2 thin-film solar cells beyond 20%, Progress in Photovoltaics 19 (2011) 894–897.
[2] W.N. Shafarman, L. Stolt, Cu(InGa)Se_2 Solar Cells, in: A. Luque, S. Hegedus (Eds.), Handbook of Photovoltaic Science and Engineering, John Wiley Sons, The Atrium, Southern Gate, Chichester, West Sussex, PO19 8SQ, United Kingdom, 2003, pp. 567–616.
[3] S.P. Udai, P.P. Surya, Progress in polycrystalline thin-film Cu(In,Ga)Se_2 solar cells, International Journal of Photoenergy 2010 (2010) 468147.
[4] N.G. Dhere, Scale-up issues of CIGS thin film PV modules, Solar Energy Material & Solar Cells 95 (2011) 277–280.
[5] T.J. McMahon, T.J. Berniard, D.S. Albin, Non-linear shunt paths in thin-film Cd–Te Solar Cells, Journal of Applied Physics 97 (2005) 054503.
[6] S. Dongaonkar, J.D. Servaites, G.M. Ford, S. Loser, J. Moore, R.M. Gelfand, H. Mohseni, H.W. Hillhouse, R. Agrawal, M.A. Retner, T.J. Marks, M. S. Lundstrom, M.A. Alam, Universality of non-Ohmic shunt leakage in thin-film solar cells, Journal of Applied Physics 108 (2010) 124509.
[7] M.A. Lampert, Volume-controlled current injection in insulators, Reports on Progress in Physics 27 (1964) 329–367.
[8] M.A. Lampert, Simplified theory of space-charge-limited currents in an insulator with traps, Physical Review 103 (1956) 1648–1656.
[9] A. Rose, Space-charge-limited currents in solids, Physical Review 97 (1955) 1538–1544.
[10] S.B. Zhang, S.H. Wei, A. Zunger, H. Katayama-Yoshida, Defect physics of the $CuInSe_2$ chalcopyrite semiconductor, Physical Review B 57 (1998) 9642–9656.
[11] ASTMG173-03, Standard Tables for Reference Solar Spectral Irradiances, ASTM International, West Conshohocken, Pennsylvania, 2003, http://dx.doi.org/10.1520/G0173-03E01, www.astm.org.
[12] K.A. Emery, C.R. Osterwald, Solar cell calibration methods, Solar Cells 27 (1989) 445–453.
[13] M.A. Contreras, J. Tuttle, A. Gabor, A. Tennant, K. Ramanathan, S. Asher, A. Franz, J. Keane, L. Wang, J. Scofield, R. Noufi, High efficiency of Cu(In,Ga)Se_2-based solar cells: processing of novel absorber structures, in: Proceeding of the 24th PVSC and WCPEC 1, 1994, pp. 68–75.
[14] M.A. Contreras, A.M. Gabor, A.L. Tennant, S. Asher, J. Tuttle, R. Noufi, 16.4% Total-area conversion efficiency thin-film polycrystalline MgF_2/ZnO/CdS/Cu(In,Ga)Se_2/Mo solar cell, Progress in Photovoltaics 2 (1994) 287–292.
[15] Z. Li, X. Yu-Ming, X. Chuan-Ming, H. Qing, L.F. Fang, L. Chang-Jian, S. Yun, Microstructural characterization of Cu(In,Ga)Se_2 surface layer, Thin Solid Films 520 (2012) 2873–2877.
[16] J.H. Park, J.M. Shin, S.Y. Cha, J.W. Park, S.Y. Jeong, H.K. Pak, C.R. Cho, Deposition-temperature effects on AZO thin films prepared by RF magnetron sputtering and their physical properties, Journal of the Korean Physical Society 49 (2006) S584–S588.
[17] J.H. Tan, W.A. Anderson, Current transport in copper indium gallium diselenide solar cells comparing mesa diodes to the full cell, Solar Energy Material & Solar Cells 77 (2003) 283–292.